ACS Chemical Neuroscience

Research Article

pubs.acs.org/chemneuro

Highly Efficient Destruction of Amyloid-β Fibrils by Femtosecond Laser-Induced Nanoexplosion of Gold Nanorods

Dongdong Lin, Ruoyu He, Shujie Li, Yongkui Xu, Jie Wang, Guanghong Wei, Minbiao Ji, and Xinju Yang*

State Key Laboratory of Surface Physics, Fudan University, Shanghai 200433, China

Collaborative Innovation Center of Advanced Microstructures, Nanjing 210093, China

Supporting Information

ABSTRACT: Alzheimer's disease (AD) is associated with the aggregation of the amyloid-beta (Aβ) peptides into toxic aggregates. How to inhibit the aggregation of Aβ peptides has been extensively studied over recent decades. The investigation on eliminating preformed fibrils, however, has rarely been reported. In this paper, near-infrared femtosecond (fs) laser is applied for the destruction of preformed Aβ fibrils in conjunction with gold nanorods (AuNRs). Our results demonstrate that the 800 nm fs-laser irradiation can locally trigger the explosion of AuNRs due to the strong localized surface plasmon resonance effect. As a result, the majority of Aβ fibrils are efficiently destroyed into small fragments by the irradiation of fs-laser with a light dose less than 75 J·cm^{-2}. Meanwhile, significant reduction of β-sheet structures is observed by thioflavin T (ThT) fluorescence measurements. In contrast, the destruction effect by continuous wave (cw) laser irradiation is much weaker with equivalent power density and irradiation time. Furthermore, the laser-induced destruction of fibrils by Au nanoparticles (AuNPs) is also investigated, which reveals that most of the Aβ fibrils remain well under the surface explosion of spherical AuNPs. Overall, our results provide a novel design for the fast destruction of amyloid fibrils locally and biocompatibly, which may have remarkable potentials in the therapy of AD.

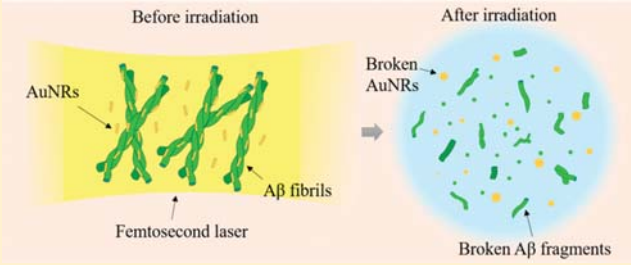

KEYWORDS: *Amyloid fibrils, destruction, gold nanorods, femtosecond laser, nanoexplosion*

The aggregation of amyloid-β peptides (Aβ) into insoluble amyloid fibrils has been considered as one of the most remarkable pathological characters of Alzheimer's disease (AD).[1−4] Previous research found that the misfolded Aβ aggregates usually consist of fibrils with a β-sheet conformation. Those accumulated Aβ aggregates finally cause the amyloid plaques in brain tissues of AD patients.[5−8] As a result, much research is aimed to explore the deep mechanism behind Aβ fibrillation process, such as the structure information on Aβ peptides and fibrils,[9−11] the inherent toxicity of aggregates,[12,13] and the structural conversion of Aβ oligomers to fibrils.[14,15] At the same time, the inhibiting of Aβ aggregates becomes a hotspot in prevention of fibrosis. Great efforts have been made in seeking amyloid inhibitors and inhibitory methods. More specifically, the inhibitory effects by nanomaterials/small molecules have been extensively studied.[16−20] For example, carbon nanomaterials (such as carbon nanotubes, fullerene, graphene, carbon dots) could suppress the aggregation of amyloid protein.[21−26] Small molecules of O_4,[15] tanshinones,[27] and hydrogen sulfide[28] were reported successively for the inhibitory effects of amyloid aggregates and the conversion of toxic oligomers to nontoxic aggregates. Besides, the effects of various nanoparticles (such as Au, Ag and copolymer) on preventing amyloid peptide aggregation have also been widely investigated.[29−31] However, the majority of the research was focused on the studies prior to the fibrillation of Aβ peptides. Few works have been reported on the investigation of preformed fibrils. In AD patients, Aβ fibrils have already formed extracellular amyloid plaques in the brain tissues. Therefore, it is critical to find ways to dissociate and eliminate the preformed fibrils.

In recent years, hyperthermia therapy has been widely used in cancer therapy, as well as in destruction of amyloid aggregates.[32,33] Hyperthermia therapy is a technique that the treatment sites are overheated to promote the selective destruction of biological targets (e.g., cancer cells, protein aggregates) by ultrasounds, microwaves and laser irradiation. For instance, high power ultrasonic treatment (UST) was applied to break amyloid-like fibrils into shorter fibrils.[34] The possibility to remotely redissolve the Aβ deposits was investigated by using microwave treatment combined with Au nanoparticles (AuNPs).[35,36] Besides, visible continuous wave laser (cw-laser) irradiation coupled with the binding of amyloid-specific thioflavin T (ThT) molecules[37,38] or AuNPs[39] was applied to destroy amyloid fibrils. In these cases, however, microwaves and UST usually require a high energy fluency because of their diffuse nature, which may produce undesirable hyperthermic effects in surrounding

Received: August 14, 2016
Accepted: September 12, 2016

DOI: 10.1021/acschemneuro.6b00244
ACS Chem. Neurosci. XXXX, XXX, XXX−XXX

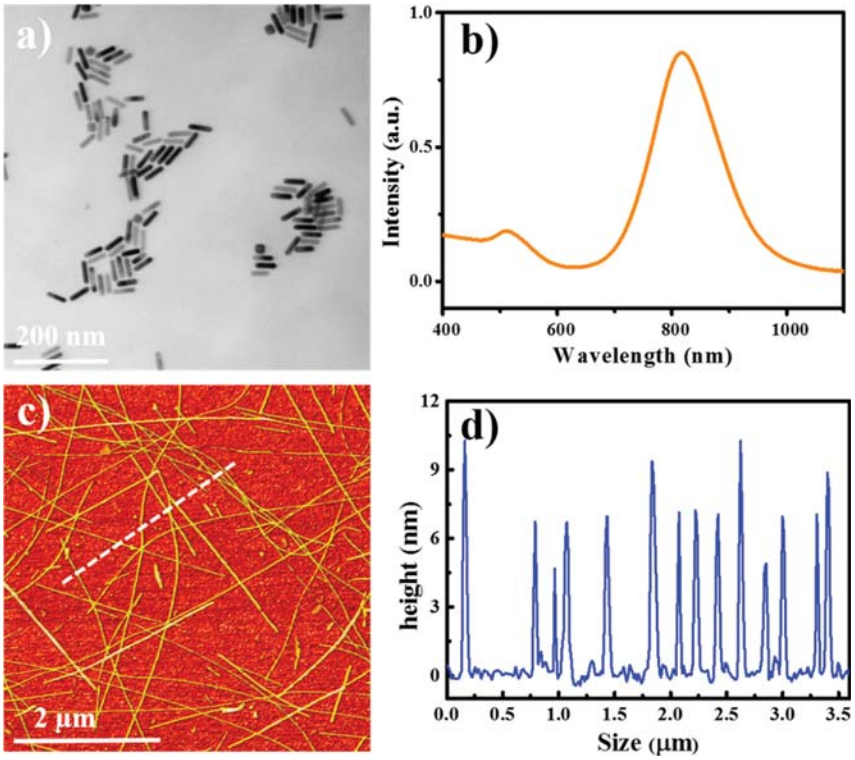

Figure 1. Characterization of synthesized AuNRs and the preformed Aβ fibrils. (a) Representative TEM image of AuNRs (40 nm × 10 nm, aspect ratio of 4). (b) UV−vis spectrum of AuNRs. (c) AFM topography image of Aβ mature fibrils incubated at 37 °C. (d) Height profile along the marked line in (c).

tissues. Additionally, the above hyperthermia therapy usually requires a long-time irradiation (hours/days) and the fibrils are partially decomposed. More to the point, laser irradiation with visible wavelengths exhibits poor penetration through tissues due to the large absorbance of tissues, and even imports extra toxicity in some cases by binding ThT molecules. Therefore, to achieve an efficient and localized destruction method, laser irradiation at near-infrared region (NIR) frequencies is preferred, because the optical window of human tissues is at 700−1000 nm.

As a better plasmonic nanomaterial, Au nanorods (AuNRs) can dramatically absorb light in the NIR with strong localized surface plasmon resonance (LSPR) in its longitudinal axis, which are more favorable in the penetration of tissues. For instance, AuNRs (aspect ratio ∼ 4) were used to diagnose and destroy cancer cell.[40] Recently, it also has been reported that a conjugate of AuNRs with the peptide CLPFFD could reduce the amyloidogenic process and its cytotoxicity by NIR cw-laser.[41] Compared to the commonly used cw-laser, pulsed laser exhibits ultrahigh transient laser power and low damage to tissues.[42,43] Previously, the computational results showed that AuNRs could be heated to a maximum temperature of 1270 K under a single fs-laser pulse with an average fluence of 4.70 J·m^{-2}.[44] With the continuous exposure of pulsed laser, the AuNRs could be exploded by the fast overheating and minimal heat diffusion.[45,46] In application, more than 90% of AuNRs-loaded cancer cells could be killed in 60 s under an unamplified fs-laser with an average light dose of 150 J·cm^{-2}, while the cw-laser at 1500 J·cm^{-2} could only result in the death of 15% of cancer cells.[47]

The experimental and computational research has greatly improved our understanding of seeking feasible methods for inhibiting and dissociating amyloid aggregates. Altogether, several issues should be concerned to improve the approaches of dissociating the prefibrillar aggregates. First, in the case of laser irradiation, the wavelength is better in the NIR region, in which the tissue has low absorption.[48] Second, the auxiliary materials for laser or microwave therapy should be non-cytotoxic. Third, the high efficiency (destruction ability, irradiation time) is preferable for the treatment. With the inspiration of surface evaporation of AuNPs by pulsed laser, we expect that the destruction effect on amyloid aggregates would be more excellent by triggering the nanoexplosion of AuNRs. In this paper, NIR femtosecond laser (fs-laser) irradiation at ∼800 nm was applied to investigate its destruction effect on mature Aβ fibrils in conjunction with AuNRs. Our results demonstrate that the irradiation of fs-laser efficiently dissociate the AuNRs loaded Aβ fibrils (Aβ fibrils@AuNRs) in 5 min at a safe energy level (unamplified fs-laser, 60−75 J·cm^{-2}). In addition, ThT fluorescence measurements indicate a significant decrease of β-sheet structures after the fs-laser irradiation. For comparison, cw-laser irradiation with the equivalent power density and irradiation time could not dissociate the Aβ fibrils. Meanwhile, guided by finite-difference-time-domain (FDTD) simulation, the destruction effects between AuNPs and AuNRs are compared, which shows that AuNRs own a much better destruction ability than the AuNPs. Finally, the cell viability results show no increase of cytotoxicity by our fs-laser-induced nanoexplosion methods. Overall, these original findings provide a potential method in the convenient and fast destruction of amyloid aggregates that related with neurodegenerative diseases.

DOI: 10.1021/acschemneuro.6b00244
ACS Chem. Neurosci. XXXX, XXX, XXX−XXX

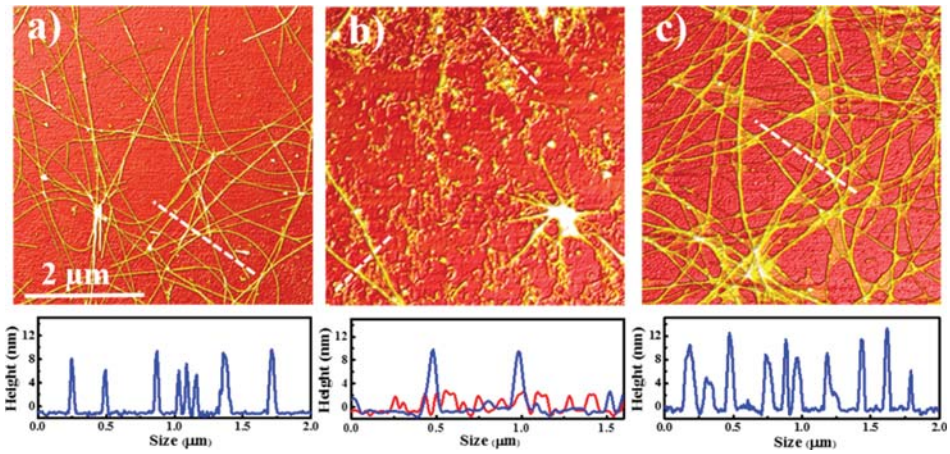

Figure 2. AFM topography images of Aβ fibrils with/without AuNRs under cw/fs laser irradiation. (a) fs-Laser treated Aβ fibrils. (b) fs-Laser treated Aβ fibrils@AuNRs. (c) cw-Laser treated Aβ fibrils@AuNRs. The corresponding height profiles are plotted under the AFM images, respectively. The irradiation wavelength is 800 nm, and the light dose is 75 J·cm^{-2}.

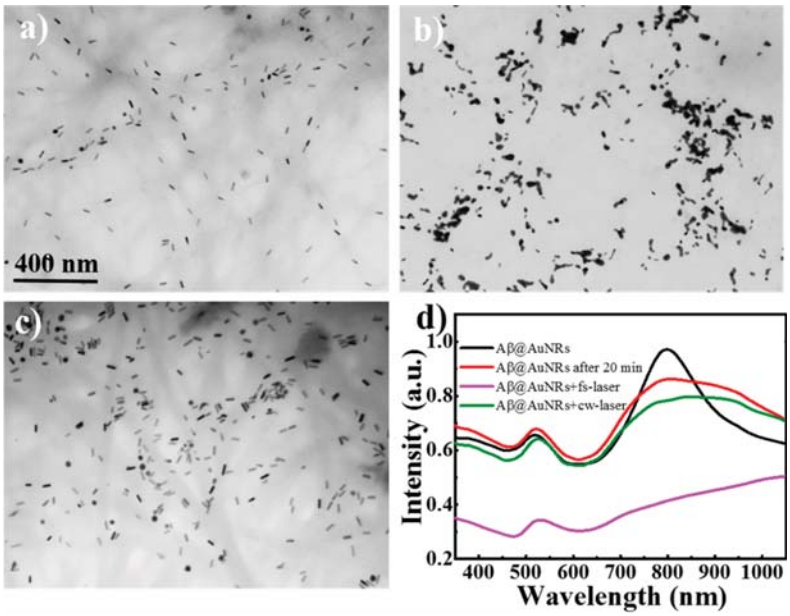

Figure 3. TEM images and UV−vis spectra of Aβ fibrils@AuNRs before/after laser irradiation. (a) TEM images of Aβ fibrils@AuNRs before laser irradiation. (b) TEM images of Aβ fibrils@AuNRs after fs-laser irradiation. (c) TEM image of Aβ fibrils@AuNRs after cw-laser irradiation. (d) UV−vis absorption spectra of AuNRs (black), Aβ fibrils@AuNRs after being incubated for 20 min (red), Aβ fibrils@AuNRs treated with fs-laser irradiation (purple), Aβ fibrils@AuNRs treated with cw-laser irradiation (green).

RESULTS AND DISCUSSION

AuNRs Dissociate the Aβ Fibrils Efficiently by fs-Laser Irradiation, While the cw-Laser Does Not. AuNRs were synthesized and applied for investigating the destruction effects on Aβ fibrils with laser irradiation. To reduce the cytotoxicity, Polyethylene glycol (PEG) was used to replace the hexadecyltrimethylammonium bromide (CTAB).[49] Previous studies reported that low concentration PEG-coated AuNRs were nontoxic in human erythrocytes[50] and colloidal gold nanoparticles were able to pass the blood−brain barrier as evident from gold concentration in the brain.[51] The synthesized AuNRs were characterized by transmission electron microscopy (TEM) image in Figure 1a. It shows that the AuNRs have uniform shapes with ∼40 nm in length and 10 nm in diameter. The aspect ratio of AuNRs is ∼4, which is reported with strong LSPR in the NIR region of ∼800 nm. The absorption spectrum of AuNRs in solution was measured by using a UV−vis spectrophotometer. A strong absorption band is located at ∼800 nm, as given in Figure 1b. To investigate the destruction effects of AuNRs on amyloid fibrils, first, Aβ fibrils were incubated using our previously reported methods.[52] The Aβ peptides were incubated for 13 days at 37 °C. As shown in Figure 1c, measured by atomic force microscopy (AFM), the length of preformed fibrils (incubated from 80 μM Aβ peptides) varies from hundred nanometers to several micrometers. The height profile along the marked line in Figure 1c reveals that the fibrils have a height of about 6−10 nm (Figure 1d).

Before the conjunction of AuNRs, we have checked the damage of fs-laser on Aβ fibrils. An unamplified fs-laser irradiation (800 nm, 6.25 nJ/pulse, 250 mW/mm^2) was performed on the bare Aβ fibril solution (610 μL, 13 μM) in

DOI: 10.1021/acschemneuro.6b00244
ACS Chem. Neurosci. XXXX, XXX, XXX−XXX

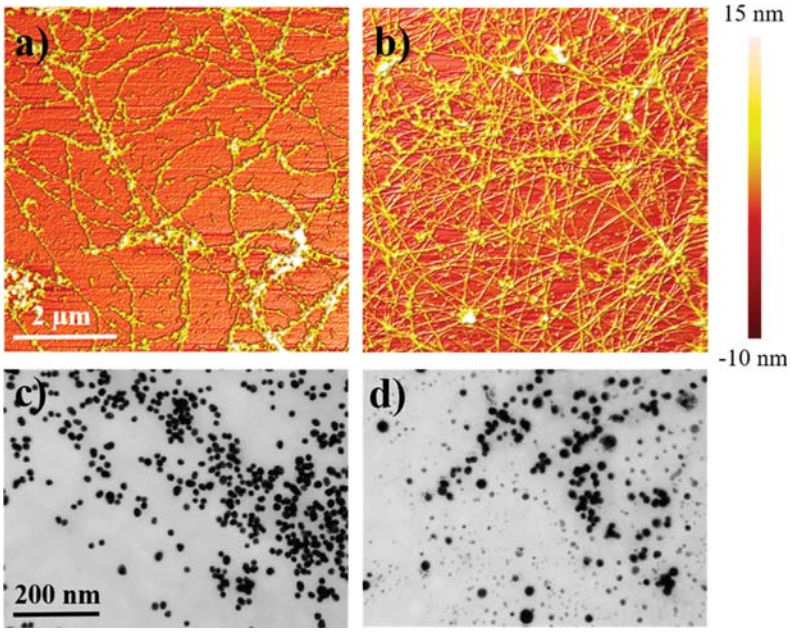

Figure 4. Representative AFM topography images and TEM images of Aβ fibrils@AuNPs before/after laser irradiation. (a) AFM image of Aβ fibrils@AuNPs. (b) AFM image of ps-laser treated Aβ fibrils@AuNPs. (c, d) Corresponding TEM images of Aβ fibrils@AuNPs and ps-laser treated Aβ fibrils@AuNPs in (a) and (b).

a quartz cuvette (10 × 10 mm^2) for 5 min. The laser spot covered the whole area by continuous scanning up and down. Consequently, a light dose of 75 J·cm^{-2} was applied in the irradiation, which has low damage to tissues and cells.[43,47] The morphology of Aβ fibrils from AFM measurement (Figure 2a) shows no obvious changes in height and length, nor the quantity of Aβ fibrils. The results indicate that a quick fs-laser exposure has no obvious broken effect on the bare Aβ fibrils. To explore the destruction ability of AuNRs on Aβ fibrils by fs-laser-induced LSPR, the prepared PEG-modified AuNRs (10 nM, 10 μL) were decorated on Aβ fibrils (80 μM, 100 μL) by physical adsorption at room temperature. From the AFM image shown in Figure S1, it clearly shows that most of AuNRs are absorbed on the surface of Aβ fibrils. Here, the fibrils become larger than that without AuNRs, this is due to the absorption of AuNRs and small Aβ aggregates on the fibrils. Then 110 μL Aβ fibrils@AuNRs solution was diluted with 500 μL water and exposed to same fs-laser irradiation (light dose of 75 J·cm^{-2}). The result shows that the majority of Aβ fibrils are broken into small fragments with a height of <3 nm (Figure 2b), which is much smaller than the height of Aβ fibrils (~6−10 nm). Only a few of long fibrils are left on substrate. In comparison, the same Aβ fibrils@AuNRs solution was irradiated by cw-laser under equivalent power density and irradiation time (Figure 2c). The AFM results are found to be much different. The majority of Aβ fibrils are not obviously damaged after the irradiation. Instead, slight laser ablation of Aβ fibrils is found, because AuNRs and their surroundings could be heated by cw-laser at 800 nm.[53]

We have also investigated the reassembling of Aβ destructed components by laser-induced nanoexplosion. The Aβ dissociated components were incubated for 10 days with the same condition that for preparing Aβ fibrils. Interestingly, the results from Figure S2a show that the number of reformed fibrils is reduced significantly. The height of reformed fibrils is still kept in less than 10 nm. At the same time, some large aggregates are absorbed on the Aβ fibrils (Figure S2b). The height of those aggregates varies from 20 to 50 nm, which is greatly higher than that of fibrils and AuNRs. Previous studies demonstrated that the protein corona (protein bound to the Au surface) affects Aβ fibrillation process.[54] We believe that, in our case, the AuNRs not only act as a nanobomb, but also serve as an inhibitor after irradiation (Au remnants) by absorbing the dissociated Aβ components and reducing the rate of Aβ fibril formation.

fs-Laser Triggers the Explosion of AuNRs. Though the efficient destruction ability on Aβ fibrils by fs-laser irradiation is obtained, the transition of AuNRs (such as shape, size, and physical properties) in Aβ fibrils@AuNRs remains to be explored. Therefore, the morphology changes of AuNRs before/after laser irradiation were studied by TEM. From Figure 3, it clearly shows that AuNRs are attached to Aβ fibrils separately before laser irradiation. Besides, the dim shadow of Aβ fibrils could be observed. When the Aβ fibrils@AuNRs were exposed to fs-laser irradiation, almost all of the AuNRs were fragmented into amorphous shapes (Figure 3b). The big plagues seem to be the fusion of exploded AuNRs, while other smaller fragments should be the remnants of exploded AuNRs. To make a comparison, the morphology of AuNRs treated with cw-laser irradiation was also measured by TEM (Figure 3c). However, the TEM image exhibits that the majority of AuNRs kept well, nor the destruction of Aβ fibrils.

In addition, UV−vis spectra were measured to investigate the dynamic plasmon absorption of AuNRs, as shown in Figure 3d. Compared with the absorption spectrum of bare AuNRs, the absorption peak at ~800 nm becomes slightly broad after the conjunction of AuNRs. When the Aβ fibrils@AuNRs were treated with fs-laser irradiation (30 J·cm^{-2}), the absorption band changed significantly. The plasmon peak at 800 nm has been destroyed dramatically, remaining with the intrinsic absorption peak of Au at ~525 nm. This dramatic change of plasmon band indicates that the fs-laser irradiation leads to the severe destruction of AuNRs. Compared to the fs-laser

DOI: 10.1021/acschemneuro.6b00244
ACS Chem. Neurosci. XXXX, XXX, XXX−XXX

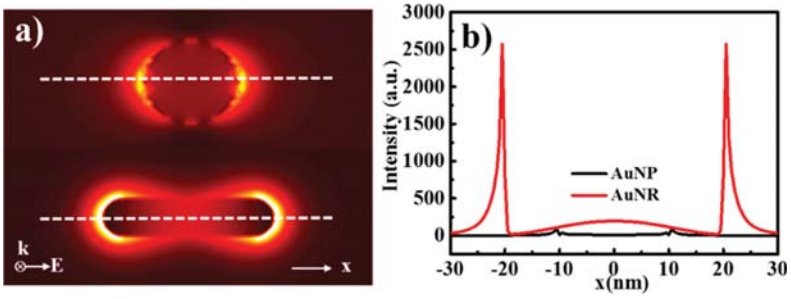

Figure 5. FDTD simulation of AuNPs and AuNRs. (a) Electric field intensity distribution of AuNPs and AuNRs. (b) Cross-sectional profiles of electric field intensity along the *x*-axis as marked in (a).

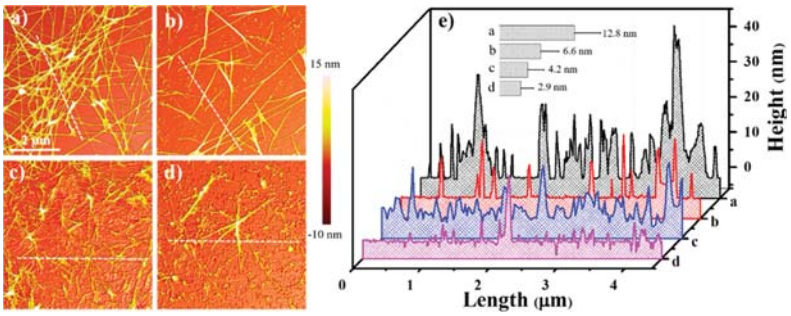

Figure 6. AFM images of Aβ fibrils@AuNRs after fs-laser irradiation at different power densities. (a) 25, (b) 50, (c) 100, and (d) 250 mW/mm^2, respectively. (e) AFM height profiles along the marked lines in (a)−(d), respectively. The average height obtained from the profiles are given in the inset.

irradiation, after the cw-laser irradiation (Figure 3d), the destruction of plasmon band is limited except a little broadening of the plasmon band at ∼800 nm, which indicates that the cw-laser irradiation with a light dose of 30 J·cm^{-2} could not cause the melting or explosion of AuNRs. Instead, the aggregation of AuNRs broadens the plasnom band.

To explain the dramatic destruction effect, the LSPR effect is considered as a major role. The electrons in AuNRs will be heated and coupled to the lattice phonons after absorbing the incident photons, then the energy of light transfers into heat. However, the increment of temperature in AuNRs depends on the balance of energy input rate and heat diffusion rate to the surrounding medium. With fs-laser irradiation, the AuNRs are heated to high enough temperature for explosion and change into other thermodynamic stable shapes, since the AuNRs lattice could not transfer the heat to surrounding water in ultimate short time period. In the case of cw-laser, as the input heat can be dissipated by surrounding timely, the input rate of heat energy is not large enough to rise the temperature to the explosion point of AuNRs. Our results are consistent with computational calculations by Strasser et al. on AuNPs by pulsed laser-induced heating. They found that for fs/ps pulsed laser, the surrounding heat diffusion is negligible. Almost all of the heat would be accumulated in AuNPs and cause the explosion of AuNPs.[55] For long pulse and cw-lasers, the heat transferred to the surrounding medium, and much lower temperature was resulted. Therefore, the above results demonstrate that the Aβ fibrils could be destroyed dramatically by triggering the explosion of AuNRs which absorbed on the Aβ fibrils, while the cw-laser has no efficient destruction effect on Aβ fibrils.

Furthermore, the destruction effect by different morphology of Au nanomaterials was investigated. The morphology image of Aβ fibrils in conjunction with AuNPs (Aβ fibrils@AuNPs) is shown in Figure 4a. It clearly shows that most of AuNPs are absorbed on the surface of Aβ fibrils. Previous studies indicated that the AuNPs could be induced in surface explosion by ns/ps pulsed laser.[45,56] Therefore, the Aβ fibrils@AuNPs were irradiated by ps-laser (532 nm, 410 μJ/pulse, 30 mW/mm^2) for 5 min. The AFM image shown in Figure 4b reveals that the irradiation causes an obvious morphology change of AuNPs but the negligible breaking of Aβ fibrils. From the corresponding TEM images shown in Figure 4c and d, it is more clearly presented that the pulsed laser triggers the surface explosion of AuNPs. The size of AuNPs was reduced and a mass of tiny gold remnants were spread on the substrate, which is in line with the previously reported results.[56] However, our results demonstrate that the surface explosion of AuNPs would not lead to the destruction of the Aβ fibrils, which may result from the relatively weak LSPR absorption that the local heating field and explosion energy are not strong enough to break the β-sheet ordered fibrils.

To explore the LSPR effects on AuNPs and AuNRs, their electric field distributions were simulated by FDTD. In comparison with AuNP, AuNR exhibits a much stronger enhancement of LSPR in longitudinal axis of AuNRs under 800 nm pulsed laser source (Figure 5a). From the profiles of electric field intensity across AuNPs and AuNRs (Figure 5b), the maximum value of electric field intensity of AuNR reaches about 28 times of the AuNP. To verify the validity of simulation, the absorption spectra of AuNP/AuNR were simulated and compared with experimental results. The absorption spectrum of AuNP/AuNR in Figure S3 shows that the simulated absorbance at 525/800 nm agrees well with the experimental results. Here, the broadened peaks in experiments are mainly due to the length fluctuation of AuNRs in fabrication. The above results indicate that the

DOI: 10.1021/acschemneuro.6b00244
ACS Chem. Neurosci. XXXX, XXX, XXX−XXX

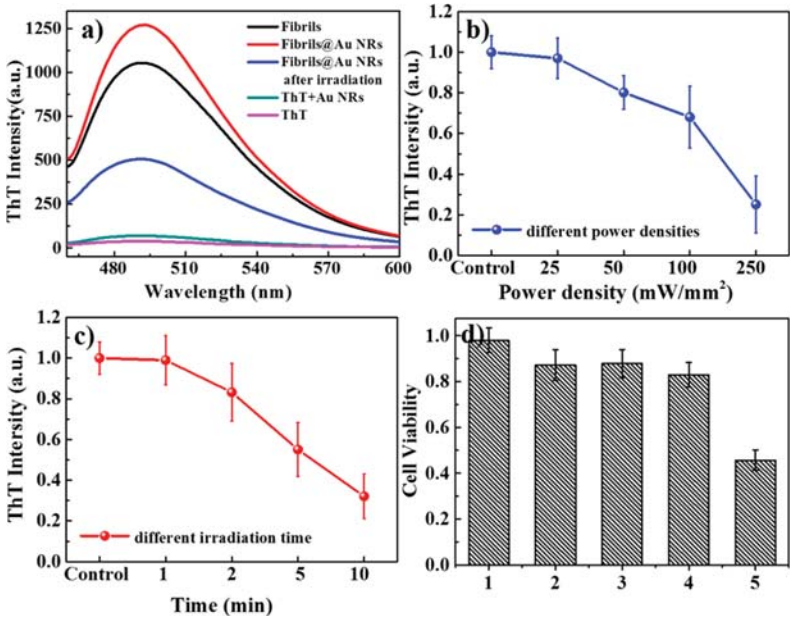

Figure 7. ThT fluorescence results on fs-laser irradiation with different power densities and irradiation time, and the cell viability measurements. (a) ThT fluorescence spectra of Aβ fibrils/Aβ fibrils@AuNRs before/after laser irradiation. (b) ThT fluorescence intensity as a function of irradiation power density. (c) ThT fluorescence intensity as a function of irradiation time. (d) Cell viability of (1) control, (2) Aβ fibrils, (3) Aβ fibrils@AuNRs, (4) Aβ fibrils@AuNRs after fs-laser irradiation, and (5) Aβ oligomers.

AuNRs are much strongly heated and exploded as nanobombs by the strong LSPR.

The Destruction Effects of Aβ Fibrils Were Dependent on fs-Laser Power Densities and Irradiation Time. In order to take deep insight into the destruction effect of AuNRs combined with fs-laser irradiation, the influence of the laser power density and irradiation time on the destruction of Aβ fibrils were investigated. Aβ fibrils@AuNRs samples were exposed to fs-laser for 5 min at different power densities of 25, 50, 100, and 250 mW/mm^2 (light doses of 7.5, 15, 30, and 75 J·cm^{-2}), respectively. The AFM images taken after each irradiation are presented in Figure 6. Clearly, no obvious destruction is observed at the power density of 25 mW/mm^2, where most of Aβ fibrils remain in long fibrils, as shown in Figure 6a. The average height of the treated fibrils reaches about 10 nm, which is displayed as the inset in Figure 6e. With the increase of laser power density, the destruction effect becomes strong. The length of broken fibrils becomes short and more fragments are generated. The average height drops to ∼6 nm with the power density increasing to 100 mW/mm^2. The strongest destruction effect is under 250 mW/mm^2 laser irradiation (Figure 6d), in which large quantities of smashing fragments are scattered on the substrate, with an average height less than 3 nm. The results clearly demonstrate that the higher laser power densities result in the more exhaustive destruction of Aβ fibrils. In addition, the destruction effect by laser irradiation (100 mW/mm^2) as a function of exposure time (1, 2, 5, and 10 min, corresponding to 6, 12, 30, and 60 J·cm^{-2}, respectively) are shown in Figure S4. For the short irradiation time of 1 and 2 min, the destruction effect is not distinct. Only a minority of fibrils are broken, and the broken fibrils aggregate into clusters (Figure S4a and b). With the increase of irradiation time, the number of broken fibrils increases gradually. For 10 min irradiation, there is almost no long fibrils left, instead of a mass of small fragments. Taken the large volume of measured sample (610 μL) into consideration, it is a high-performance result by minute-scanned area of 10 × 10 mm^2.

The Irradiation of fs-Laser Reduces the β-Sheet Structure Dramatically, But without Increasing the Cytotoxicity. The conformational changes of Aβ fibrils by fs-laser irradiation were measured by thioflavin T (ThT) fluorescence assay. ThT fluorescence assay is widely used in detecting β-sheet structure in amyloid protein aggregation, as the ThT molecules can be bound to β-sheet structure specifically.[57,58] Figure 7a presents the ThT fluorescence spectra of AuNRs, Aβ fibrils, and Aβ fibrils@AuNPs before and after laser irradiation. It can be clearly seen that all the spectra have a large peak at ∼490 nm which is related with ordered β-sheet structures in Aβ fibrils. The fluorescence signal shows a slight increase for Aβ fibrils@AuNRs sample, probably due to the AuNRs can enhance the ThT fluorescence. However, the ThT signal decreases dramatically after fs-laser irradiation (30 J·cm^{-2}), indicating the large decrease of β-sheet-rich fibrils. Our method provides an opposite result in dissociating fibrils compared with UST and microwave treatments, which would increase the ThT fluorescence intensity inversely.[34,36] As describe in UST method, it mechanically cut the long fibrils into short ones, which increases the number of fibril ends.[34] In our case, the fs-laser irradiation not only breaks β-sheet-rich fibrils to ultratiny fragments, but also destroys the β-sheet structures. Similar ThT results have been reported by long-time cw-laser irradiation with AuNRs.[37] In addition, the ThT intensity of Aβ fibrils@AuNRs as a function of laser power density and laser irradiation time are measured and shown in Figure 7b and c, which corresponds to the AFM results in Figures 6 and S3. Obviously, the intensity of ThT fluorescence reduces significantly with the increase of laser power density, reaching the lowest of 22% at the light dose of 75 J·cm^{-2}. Besides, with the increase of irradiation time, the sample has a linear decreasing of ThT fluorescence intensity. Almost 70% of ThT fluorescence

DOI: 10.1021/acschemneuro.6b00244
ACS Chem. Neurosci. XXXX, XXX, XXX−XXX

intensity is reduced after the irradiation of 5 min (60 J·cm^{-2}), which is consistent with the results by AFM observation. Compared to cw-laser irradiation (450 mW) with AuNRs,[41] in which the decrease of ThT fluorescence intensity after 2 h irradiation was about 40%, fs-laser irradiation induced nanoexplosion fulfils a much higher destruction efficiency with low power density and short exposure time.

Having shown that AuNRs have high efficient on dissociating Aβ fibrils under the irradiation of fs-laser, we finally measured the cytotoxicity of laser treated products on the neuroblastoma cells (SH-SY5Y). As presented in Figure 7d (1−5 represent control, Aβ fibrils, Aβ fibrils@AuNRs, Aβ fibrils@AuNRs irradiated by fs-laser, and Aβ oligomers, respectively), the results indicate that the cytotoxicity of Aβ fibrils@AuNRs complex is almost equal to that of bare Aβ fibrils, having an ∼87% survival rate. After being treated with fs-laser irradiation (75 J·cm^{-2}), the cell viability of Aβ fibrils@AuNRs still keeps in the same level, reaching to ∼84%. The slight drop of cell viability might be attributed to the existence/reformation of toxic oligomers, as the reassembly results further reveal that few Aβ fibrils would be reformed. However, compared with the toxic Aβ oligomers (40% survival rate), our fs-laser treated components exhibit low toxicity, which indicates the destructive products are not the toxic Aβ oligomers. Although the cell viability is not improved compared to the low toxic mature fibrils, we provide a method for the efficient destruction of Aβ fibrils, which might have important potentials for the therapy of AD.

CONCLUSION

In summary, a novel method in dissociating Aβ fibrils is introduced. With the measurements of AFM, TEM, UV−vis and ThT fluorescence assay, our results demonstrate that Aβ fibrils in conjunction with AuNRs can be efficiently destroyed under fs-laser irradiation without increasing the cytotoxicity. The fs-laser can trigger the nanoexplosion of AuNRs by LSPR locally, and break the Aβ fibrils into non-β-sheet structure components drastically. The fibrils destruction effect becomes stronger with the increase of irradiation time and laser power densities. In comparison, a cw-laser irradiation with equivalent condition cannot break the fibrils in such a short time scale. In addition, the destruction effects are much weaker by the explosion of AuNPs. Overall, our findings provide a potential method in the therapy of AD and related amyloid diseases with high-efficient and biocompatible destruction of aggregates.

METHODS

Incubation of Aβ fibrils. Aβ peptides were purchased from Chinese Peptide Ltd. (Hangzhou, China). The final purity was greater than 98%. Aβ peptides solution was prepared by dissolving the peptide powder in phosphate-buffered saline (PBS) buffer and incubated at 37 °C to oligomers (1 h) and mature fibrils (∼10 days).

Synthesis of PEG-AuNRs. AuNRs were synthesized using a seed-mediated approach as reported in our work.[59] First, to synthesize gold nanoseeds, 125 μL of $HAuCl_4$ (20 mM) and 7.5 mL of CTAB (0.1 M) were gently mixed in a 10 mL glass bottle. Then 0.6 mL of ice-bathed $NaBH_4$ solution (10 mM) was injected, with magnetic stirring until the color changed from golden yellow to brown. The seed solution was kept at 27 °C for 2 h before use. Second, 250 μL of $HAuCl_4$ (20 mM) and 100 μL of $AgNO_3$ (10 mM) were added into 10 mL of CTAB (0.1 M) in a glass bottle. After that, L-ascorbic acid (0.1 M, 60 μL) and the 10 times diluted gold nanoseeds (120 μL) were gently injected with an aqueous bath. Finally, the solution was left at 27 °C overnight to grow CTAB stabilized Au NR. PEG-modified AuNRs were prepared with phosphatidylcholine (PC) followed with the methods reported by Niidome et al.[49] The products were isolated by centrifugation at 15 000 rpm for 10 min to remove the redundant CTAB. Then 1 mg PEG-SH was added to 15 mL preprepared AuNRs solution and stirred for 2 h. The final PEG-modified AuNRs were collected by twice centrifugation at 10,000 rpm for 30 min.

Sample Preparation and AFM/TEM Characterization. The Aβ fibrils@AuNRs samples were prepared by mixing 10 μL AuNRs (1 nM) with 100 μL Aβ fibrils solution (incubated from 80 μM Aβ peptide solution), and oscillated by vortex mixer for 1 min. The morphology change of Aβ fibrils@AuNRs was observed by AFM and TEM. To prepare samples for AFM imaging, an aliquot of 3 μL of Aβ fibrils@AuNRs solution was deposited on the freshly cleaved mica surface (1 × 1 cm^2). The deposited droplet was dried under a gentle stream of nitrogen, and measured by AFM (Multimode V, Bruker Surface Nano) in tapping mode immediately. For TEM imaging, 5 μL of Aβ fibrils@AuNRs solution was deposited on the carbon coated copper grids, and then measured with a JEM-2100 TEM at an accelerating voltage of 200 kV. The preparation of Aβ fibrils@AuNPs sample was in the same way except one more step of gentle ultrasonic separation, as they cause the aggregation of fibrils quickly.

Laser Irradiation. Femtosecond pulsed laser (Insight DeepSee Laser System, 680−1300 nm) with pulse width of ∼120 fs and pulse repetition of 80 MHz was used in this study. In irradiation experiments, 110 μL of Aβ fibrils@AuNRs aqueous solution was diluted in 500 μL of water and transferred to a 10 mm × 10 mm quartz cuvette. The Aβ fibrils@AuNRs samples were irradiated by the fs-laser at 800 nm with an unfocused spot diameter of about 1.6 mm. For comparison, cw-laser at 800 nm with same power density was used. The laser beam direction to quartz cuvette was designed from top of the quartz cuvette to bottom to avoid the depletion of laser beam and liquid outflow. The quartz cuvette kept scanning to ensure the whole sample would be covered in irradiation. For 5 min fs-irradiation at the maximum power density of 250 mW/mm^2, a light does of 75 J·cm^{-2} can be roughly estimated. For the comparative experiments with AuNPs, a 532 nm picosecond pulse laser (20 Hz, 30 ps, 410 μJ/pulse) was used with the spot diameter about 0.6 mm.

ThT Fluorescence and UV/Vis Absorption Measurements. The ThT fluorescence measurements were performed with F-2500 FL spectrophotometer (Hitachi) at room temperature by using an excitation wavelength at 440 nm and emission wavelength at 485 nm, as well as the excitation and emission slits of 5 nm.[26] The measured samples were prepared by mixing 100 μL Aβ fibrils@AuNRs solution with 10 μL ThT (1 mM) and 890 μL PBS solutions in a 10 mm quartz cell. For comparison, the ThT control sample was prepared by mixing 10 μL ThT (1 mM) solution with 990 μL PBS solution. Every group was repeated with five separate samples under same condition. For UV−vis absorption measurement, an Agilent 8453 UV−vis spectrophotometer with microquartz cuvettes of 10 mm optical path length was used.

Cytotoxicity Measurements. SH-SY5Y cells were treated in DMEM medium with 10% calf serum, 100 units/mL penicillin, 100 μg/mL streptomycin, and 100 μg/mL neomycin in a humidified standard incubator. The temperature is kept at 37 °C, with a 5% CO_2 atmosphere. After incubation, the cells were washed with PBS solution for three times to remove the unassociated compounds and replenished with fresh medium. When the cells reached 80% confluence, 20 μL of Aβ fibrils, AuNRs, and Aβ fibrils@AuNRs before/after irradiation were added in wells and incubated for 3 h. Finally, 10 μL of WST-1 solution (5 mg/mL) was added into each well for incubation of another 2 h. Samples were measured on an iEMS Analyzer (Lab-system) at 450 nm of each well. The cell viability in each well was calculated by comparing the optical densities (O.D) value with that of untreated cells in the same condition. All results were presented as the mean ± standard error (SE) from three independent experiments with five wells in each.

Finite-Difference-Time-Domain (FDTD) Simulation. We used Lumerical FDTD Solution (version 8.12.590) to perform FDTD simulation. The Au NP and Au NR were placed in water medium. The optical data of gold is from Johnson and Christy.[60] The source with

DOI: 10.1021/acschemneuro.6b00244
ACS Chem. Neurosci. XXXX, XXX, XXX−XXX

polarization angle of 0° was incident from top of Au NP/Au NR. Polarization angle of 45° was set for the simulation of absorption spectra. Meshing enclosing the entire model was set to 0.25/0.5 nm per grid. The *x*-, *y*-, and *z*-axis boundaries of the simulation region were set to Perfect Matching Layer. A *z*-normal 2D monitor was placed for absorption spectra. Near-field cross-sectional electrical intensity profiles was obtained by a *z*-normal 2D monitor passing the rods axis.

■ ASSOCIATED CONTENT

Supporting Information

The Supporting Information is available free of charge on the ACS Publications website at DOI: 10.1021/acschemneuro.6b00244.

AFM topography images of Aβ fibrils@AuNRs before irradiation, reformed Aβ fibrils after fs-laser irradiation, adsorption spectrum of AuNP and AuNR from experiment and FDTD simulation, AFM images of fs-laser treated Aβ fibrils@AuNRs as a function of irradiation time (PDF)

■ AUTHOR INFORMATION

Corresponding Author

*Mailing address: Department of Physics, Fudan University, 220 Handan Road, Shanghai 200433, China. Tel: +86 21 55665337. E-mail: xjyang@fudan.edu.cn.

Author Contributions

D.L. and X.Y. designed the research; D.L., R.H., and S.L. performed experimental research; J.W. and G.W. performed simulation; D.L., M. J., G.W., and X.Y. analyzed data; D.L. and X.Y. wrote the paper.

Funding

This work was supported by National Natural Science Foundation of China (No. 11274072). G.W. acknowledges the financial support from NSF of China (Grant No. 11274075).

Notes

The authors declare no competing financial interest.

■ ABBREVIATIONS

AD, Alzheimer's disease; Aβ, amyloid-β peptides; AuNRs, gold nanorods; Au NPs, gold nanoparticles; fs-laser, femtosecond laser; ps-laser, picosecond laser; cw, continuous wave; UST, ultrasonic treatment; PEG, polyethylene glycol; UV−vis, ultraviolet−visible-near-infrared spectrophotometer; ThT, thioflavin T; AFM, atomic force microscopy; TEM, transmission electrostatic microscopy; FDTD, finite-difference-time-domain

■ REFERENCES

(1) Selkoe, D. J. (1989) Amyloid β protein precursor and the pathogenesis of Alzheimer's disease. *Cell 58*, 611−612.

(2) Eisenberg, D., and Jucker, M. (2012) The Amyloid State of Proteins in Human Diseases. *Cell 148*, 1188−1203.

(3) Lorenzo, A., Yuan, M., Zhang, Z., Paganetti, P. A., Sturchler-Pierrat, C., Staufenbiel, M., Mautino, J., Vigo, F. S., Sommer, B., and Yankner, B. A. (2000) Amyloid [beta] interacts with the amyloid precursor protein: a potential toxic mechanism in Alzheimer's disease. *Nat. Neurosci. 3*, 460−464.

(4) LaFerla, F. M., Green, K. N., and Oddo, S. (2007) Intracellular amyloid-beta in Alzheimer's disease. *Nat. Rev. Neurosci. 8*, 499−509.

(5) Chiti, F., and Dobson, C. M. (2006) Protein misfolding, functional amyloid, and human disease. *Annu. Rev. Biochem. 75*, 333−66.

(6) Hardy, J., and Selkoe, D. J. (2002) Medicine - The amyloid hypothesis of Alzheimer's disease: Progress and problems on the road to therapeutics. *Science 297*, 353−356.

(7) Ross, C. A., and Poirier, M. A. (2004) Protein aggregation and neurodegenerative disease. *Nat. Med. 10* (Suppl), S10−7.

(8) Hardy, J., and Selkoe, D. J. (2002) The amyloid hypothesis of Alzheimer's disease: progress and problems on the road to therapeutics. *Science 297*, 353−6.

(9) Lu, J.-X., Qiang, W., Yau, W.-M., Schwieters, C. D., Meredith, S. C., and Tycko, R. (2013) Molecular Structure of β-Amyloid Fibrils in Alzheimer's Disease Brain Tissue. *Cell 154*, 1257−1268.

(10) Petkova, A. T., Ishii, Y., Balbach, J. J., Antzutkin, O. N., Leapman, R. D., Delaglio, F., and Tycko, R. (2002) A structural model for Alzheimer's beta -amyloid fibrils based on experimental constraints from solid state NMR. *Proc. Natl. Acad. Sci. U. S. A. 99*, 16742−7.

(11) Ma, B., and Nussinov, R. (2002) Stabilities and conformations of Alzheimer's beta -amyloid peptide oligomers (Abeta 16−22, Abeta 16−35, and Abeta 10−35): Sequence effects. *Proc. Natl. Acad. Sci. U. S. A. 99*, 14126−31.

(12) Laganowsky, A., Liu, C., Sawaya, M. R., Whitelegge, J. P., Park, J., Zhao, M., Pensalfini, A., Soriaga, A. B., Landau, M., Teng, P. K., Cascio, D., Glabe, C., and Eisenberg, D. (2012) Atomic view of a toxic amyloid small oligomer. *Science 335*, 1228−31.

(13) Bucciantini, M., Giannoni, E., Chiti, F., Baroni, F., Formigli, L., Zurdo, J., Taddei, N., Ramponi, G., Dobson, C. M., and Stefani, M. (2002) Inherent toxicity of aggregates implies a common mechanism for protein misfolding diseases. *Nature 416*, 507−11.

(14) Ahmed, M., Davis, J., Aucoin, D., Sato, T., Ahuja, S., Aimoto, S., Elliott, J. I., Van Nostrand, W. E., and Smith, S. O. (2010) Structural conversion of neurotoxic amyloid-beta(1−42) oligomers to fibrils. *Nat. Struct. Mol. Biol. 17*, 561−7.

(15) Bieschke, J., Herbst, M., Wiglenda, T., Friedrich, R. P., Boeddrich, A., Schiele, F., Kleckers, D., Lopez del Amo, J. M., Grüning, B. A., Wang, Q., Schmidt, M. R., Lurz, R., Anwyl, R., Schnoegl, S., Fändrich, M., Frank, R. F., Reif, B., Günther, S., Walsh, D. M., and Wanker, E. E. (2012) Small-molecule conversion of toxic oligomers to nontoxic β-sheet−rich amyloid fibrils. *Nat. Chem. Biol. 8*, 93−101.

(16) Li, C., and Mezzenga, R. (2013) The interplay between carbon nanomaterials and amyloid fibrils in bio-nanotechnology. *Nanoscale 5*, 6207−18.

(17) Härd, T., and Lendel, C. (2012) Inhibition of Amyloid Formation. *J. Mol. Biol. 421*, 441−465.

(18) Nie, Q., Du, X.-g., and Geng, M.-y. (2011) Small molecule inhibitors of amyloid [beta] peptide aggregation as a potential therapeutic strategy for Alzheimer's disease. *Acta Pharmacol. Sin. 32*, 545−551.

(19) Porat, Y., Abramowitz, A., and Gazit, E. (2006) Inhibition of Amyloid Fibril Formation by Polyphenols: Structural Similarity and Aromatic Interactions as a Common Inhibition Mechanism. *Chem. Biol. Drug Des. 67*, 27−37.

(20) Zhang, M., Mao, X., Yu, Y., Wang, C.-X., Yang, Y.-L., and Wang, C. (2013) Nanomaterials for Reducing Amyloid Cytotoxicity. *Adv. Mater. 25*, 3780−3801.

(21) Ghule, A. V., Kathir, K. M., Suresh Kumar, T. K., Tzing, S.-H., Chang, J.-Y., Yu, C., and Ling, Y.-C. (2007) Carbon nanotubes prevent 2,2,2 trifluoroethanol induced aggregation of protein. *Carbon 45*, 1586−1589.

(22) Zhou, X., Xi, W., Luo, Y., Cao, S., and Wei, G. (2014) Interactions of a Water-Soluble Fullerene Derivative with Amyloid-β Protofibrils: Dynamics, Binding Mechanism, and the Resulting Salt-Bridge Disruption. *J. Phys. Chem. B 118*, 6733−6741.

(23) Ge, C., Du, J., Zhao, L., Wang, L., Liu, Y., Li, D., Yang, Y., Zhou, R., Zhao, Y., Chai, Z., and Chen, C. (2011) Binding of blood proteins to carbon nanotubes reduces cytotoxicity. *Proc. Natl. Acad. Sci. U. S. A. 108* (41), 16968−16973.

(24) Xie, L., Luo, Y., Lin, D., Xi, W., Yang, X., and Wei, G. (2014) The molecular mechanism of fullerene-inhibited aggregation of Alzheimer's beta-amyloid peptide fragment. *Nanoscale 6*, 9752−9762.

DOI: 10.1021/acschemneuro.6b00244
ACS Chem. Neurosci. XXXX, XXX, XXX−XXX

(25) Li, S., Wang, L., Chusuei, C. C., Suarez, V. M., Blackwelder, P. L., Micic, M., Orbulescu, J., and Leblanc, R. M. (2015) Nontoxic Carbon Dots Potently Inhibit Human Insulin Fibrillation. *Chem. Mater. 27*, 1764−1771.
(26) Lin, D., Qi, R., Li, S., He, R., Li, P., Wei, G., and Yang, X. (2016) The interaction dynamics in inhibiting the aggregation of Aβ peptides by SWCNTs: a combined experimental and coarse-grained molecular dynamic simulations study. *ACS Chem. Neurosci.*, DOI: 10.1021/acschemneuro.6b00101.
(27) Wang, Q., Yu, X., Patal, K., Hu, R., Chuang, S., Zhang, G., and Zheng, J. (2013) Tanshinones Inhibit Amyloid Aggregation by Amyloid-β Peptide, Disaggregate Amyloid Fibrils, and Protect Cultured Cells. *ACS Chem. Neurosci. 4*, 1004−1015.
(28) Rosario-Alomar, M. F., Quiñones-Ruiz, T., Kurouski, D., Sereda, V., Ferreira, E. B., Jesús-Kim, L. D., Hernández-Rivera, S., Zagorevski, D. V., López-Garriga, J., and Lednev, I. K. (2015) Hydrogen Sulfide Inhibits Amyloid Formation. *J. Phys. Chem. B 119*, 1265−1274.
(29) Linse, S., Cabaleiro-Lago, C., Xue, W. F., Lynch, I., Lindman, S., Thulin, E., Radford, S. E., and Dawson, K. A. (2007) Nucleation of protein fibrillation by nanoparticles. *Proc. Natl. Acad. Sci. U. S. A. 104*, 8691−6.
(30) Anand, B. G., Dubey, K., Shekhawat, D. S., and Kar, K. (2016) Capsaicin-Coated Silver Nanoparticles Inhibit Amyloid Fibril Formation of Serum Albumin. *Biochemistry 55*, 3345−3348.
(31) Cabaleiro-Lago, C., Szczepankiewicz, O., and Linse, S. (2012) The Effect of Nanoparticles on Amyloid Aggregation Depends on the Protein Stability and Intrinsic Aggregation Rate. *Langmuir 28*, 1852−1857.
(32) Huff, T. B., Tong, L., Zhao, Y., Hansen, M. N., Cheng, J.-X., and Wei, A. (2007) Hyperthermic effects of gold nanorods on tumor cells. *Nanomedicine (London, U. K.) 2*, 125−132.
(33) Li, M., Yang, X., Ren, J., Qu, K., and Qu, X. (2012) Using Graphene Oxide High Near-Infrared Absorbance for Photothermal Treatment of Alzheimer's Disease. *Adv. Mater. 24*, 1722−1728.
(34) Lee, W., Jung, H., Son, M., Lee, H., Kwak, T. J., Lee, G., Kim, C. H., Lee, S. W., and Yoon, D. S. (2014) Characterization of the regrowth behavior of amyloid-like fragmented fibrils decomposed by ultrasonic treatment. *RSC Adv. 4*, 56561−56566.
(35) Bastus, N. G., Kogan, M. J., Amigo, R., Grillo-Bosch, D., Araya, E., Turiel, A., Labarta, A., Giralt, E., and Puntes, V. F. (2007) Gold nanoparticles for selective and remote heating of β-amyloid protein aggregates. *Mater. Sci. Eng., C 27*, 1236−1240.
(36) Kogan, M. J., Bastus, N. G., Amigo, R., Grillo-Bosch, D., Araya, E., Turiel, A., Labarta, A., Giralt, E., and Puntes, V. F. (2006) Nanoparticle-Mediated Local and Remote Manipulation of Protein Aggregation. *Nano Lett. 6*, 110−115.
(37) Ozawa, D., Kaji, Y., Yagi, H., Sakurai, K., Kawakami, T., Naiki, H., and Goto, Y. (2011) Destruction of amyloid fibrils of keratoepithelin peptides by laser irradiation coupled with amyloid-specific thioflavin T. *J. Biol. Chem. 286*, 10856−63.
(38) Yagi, H., Ozawa, D., Sakurai, K., Kawakami, T., Kuyama, H., Nishimura, O., Shimanouchi, T., Kuboi, R., Naiki, H., and Goto, Y. (2010) Laser-induced propagation and destruction of amyloid beta fibrils. *J. Biol. Chem. 285*, 19660−7.
(39) Triulzi, R. C., Dai, Q., Zou, J., Leblanc, R. M., Gu, Q., Orbulescu, J., and Huo, Q. (2008) Photothermal ablation of amyloid aggregates by gold nanoparticles. *Colloids Surf., B 63*, 200−8.
(40) Huang, X., El-Sayed, I. H., Qian, W., and El-Sayed, M. A. (2006) Cancer Cell Imaging and Photothermal Therapy in the Near-Infrared Region by Using Gold Nanorods. *J. Am. Chem. Soc. 128*, 2115−2120.
(41) Adura, C., Guerrero, S., Salas, E., Medel, L., Riveros, A., Mena, J., Arbiol, J., Albericio, F., Giralt, E., and Kogan, M. J. (2013) Stable Conjugates of Peptides with Gold Nanorods for Biomedical Applications with Reduced Effects on Cell Viability. *ACS Appl. Mater. Interfaces 5*, 4076−4085.
(42) Vogel, A., and Venugopalan, V. (2003) Mechanisms of Pulsed Laser Ablation of Biological Tissues. *Chem. Rev. 103*, 577−644.
(43) Hashmi, J. T., Huang, Y.-Y., Sharma, S. K., Kurup, D. B., De Taboada, L., Carroll, J. D., and Hamblin, M. R. (2010) Effect of Pulsing in Low-Level Light Therapy. *Lasers Surg. Med. 42*, 450−466.
(44) Ekici, O., Harrison, R. K., Durr, N. J., Eversole, D. S., Lee, M., and Ben-Yakar, A. (2008) Thermal analysis of gold nanorods heated with femtosecond laser pulses. *J. Phys. D: Appl. Phys. 41*, 185501.
(45) Letfullin, R. R., Joenathan, C., George, T. F., and Zharov, V. P. (2006) Laser-induced explosion of gold nanoparticles: potential role for nanophotothermolysis of cancer. *Nanomedicine 1*, 473−480.
(46) Link, S., Burda, C., Nikoobakht, B., and El-Sayed, M. A. (2000) Laser-Induced Shape Changes of Colloidal Gold Nanorods Using Femtosecond and Nanosecond Laser Pulses. *J. Phys. Chem. B 104*, 6152−6163.
(47) Wu, X., Chen, J.-Y., Brech, A., Fang, C., Wang, J., Helm, P. J., and Peng, Q. (2013) The use of femto-second lasers to trigger powerful explosions of gold nanorods to destroy cancer cells. *Biomaterials 34*, 6157−6162.
(48) Sordillo, L. A., Pu, Y., Pratavieira, S., Budansky, Y., and Alfano, R. R. (2014) Deep optical imaging of tissue using the second and third near-infrared spectral windows. *J. Biomed. Opt. 19*, 056004.
(49) Niidome, T., Yamagata, M., Okamoto, Y., Akiyama, Y., Takahashi, H., Kawano, T., Katayama, Y., and Niidome, Y. (2006) PEG-modified gold nanorods with a stealth character for in vivo applications. *J. Controlled Release 114*, 343−347.
(50) Lau, I. P., Chen, H., Wang, J., Ong, H. C., Leung, K. C. F., Ho, H. P., and Kong, S. K. (2012) In vitro effect of CTAB- and PEG-coated gold nanorods on the induction of eryptosis/erythroptosis in human erythrocytes. *Nanotoxicology 6*, 847−856.
(51) Sonavane, G., Tomoda, K., and Makino, K. (2008) Biodistribution of colloidal gold nanoparticles after intravenous administration: Effect of particle size. *Colloids Surf., B 66*, 274−280.
(52) Lin, D., Luo, Y., Wu, S., Ma, Q., Wei, G., and Yang, X. (2014) Investigation of the aggregation process of amyloid-beta-(16−22) peptides and the dissolution of intermediate aggregates. *Langmuir 30*, 3170−5.
(53) Mahmoudi, M., Lohse, S. E., Murphy, C. J., Fathizadeh, A., Montazeri, A., and Suslick, K. S. (2014) Variation of Protein Corona Composition of Gold Nanoparticles Following Plasmonic Heating. *Nano Lett. 14*, 6−12.
(54) Mirsadeghi, S., Dinarvand, R., Ghahremani, M. H., Hormozi-Nezhad, M. R., Mahmoudi, Z., Hajipour, M. J., Atyabi, F., Ghavami, M., and Mahmoudi, M. (2015) Protein corona composition of gold nanoparticles/nanorods affects amyloid beta fibrillation process. *Nanoscale 7*, 5004−5013.
(55) Strasser, M., Setoura, K., Langbein, U., and Hashimoto, S. (2014) Computational Modeling of Pulsed Laser-Induced Heating and Evaporation of Gold Nanoparticles. *J. Phys. Chem. C 118*, 25748−25755.
(56) Hashimoto, S., Werner, D., and Uwada, T. (2012) Studies on the interaction of pulsed lasers with plasmonic gold nanoparticles toward light manipulation, heat management, and nanofabrication. *J. Photochem. Photobiol., C 13*, 28−54.
(57) Khurana, R., Coleman, C., Ionescu-Zanetti, C., Carter, S. A., Krishna, V., Grover, R. K., Roy, R., and Singh, S. (2005) Mechanism of thioflavin T binding to amyloid fibrils. *J. Struct. Biol. 151*, 229−38.
(58) Biancalana, M., and Koide, S. (2010) Molecular mechanism of Thioflavin-T binding to amyloid fibrils. *Biochim. Biophys. Acta, Proteins Proteomics 1804*, 1405−12.
(59) Xu, Y., He, R., Lin, D., Ji, M., and Chen, J. (2015) Laser beam controlled drug release from Ce6-gold nanorod composites in living cells: a FLIM study. *Nanoscale 7*, 2433−41.
(60) Johnson, P. B., and Christy, R. W. (1972) Optical Constants of the Noble Metals. *Phys. Rev. B 6*, 4370−4379.

DOI: 10.1021/acschemneuro.6b00244
ACS Chem. Neurosci. XXXX, XXX, XXX−XXX